Progress In Electromagnetics Research M, Vol. 118, 11–23, 2023

Four-Port UWB MIMO Vivaldi Antenna Based on Resistor and Radiant Patch

Jingchang Nan, Huimei Zhang*, and Jv Huang

Abstract—A four-port ultra-wideband (UWB) multi-input multi-output (MIMO) Vivaldi antenna loaded with resistance and rectangular radiation patch is designed and fabricated. The compact antenna consists of an improved ground and four microstrip feeders, with an overall size of 26 mm × 52 mm × 0.8 mm. The antenna adopts the resistance loading technology to absorb the excess electromagnetic waves in the low-frequency band and broaden the low-frequency bandwidth of the antenna. The rectangular radiation patch loading technique optimizes the main radiation direction and broadens the high-frequency bandwidth of the antenna. Meanwhile, T-slots and fence-type structures are etched on the ground plane, and I-stubs are added between microstrip feeders to reduce the antenna coupling and increase the isolation degree between the antenna ports. Simulation and experiments show that the impedance bandwidth of the MIMO antenna is 3.0 ∼ 12.3 GHz; the isolation degree of the whole working bandwidth is higher than 15 dB; the envelope correlation coefficient (ECC) is smaller than 0.43; and the increased diversity gain (DG) is more significant than 9.98 dBi. The antenna has good radiation performance and stable gain, which is suitable for applying the UWB MIMO system. This antenna has a particular reference significance for the research of the MIMO Vivaldi antenna.

1. INTRODUCTION

Wireless communication technology is developing rapidly, and ultra-wideband (UWB) technology [1–3] has been widely studied because of its high transmission rate, strong interference immunity, and ease of fabrication. Although UWB technology has significant advantages, it also faces problems such as reliability and multipath fading. As a result, multiple-input multiple-output (MIMO) technology [4] has emerged. MIMO technology is a diverse technology using multiple transmitting and receiving antennas. This technology can transform multipath fading, which is unfavorable to wireless communication transmission, into a favorable factor that improves the reliability of data transmission in the system. Combining UWB and MIMO technology [5–9] can improve data transmission efficiency and suppress the multipath effect. It can also improve the quality and capacity of communication.

MIMO antenna systems must ensure small size and low mutual coupling to be compatible with modern portable small communication devices. Various decoupling structures [10–21] have been used to reduce the mutual coupling of MIMO antennas under the condition that the antenna size is fixed. In [10], a new type of barrier decoupling structure was proposed; by introducing a palisade decoupling structure on the ground surface of the antenna and an I-type branch between the antenna radiation units, the working band isolation of the antenna was enhanced. In [11], a T-slot was etched between two tapered gaps to improve the isolation of the antenna. In [12], a new ITI decoupling structure was designed and placed in the middle of the patch antenna. At the same time, an asymmetric defective ground structure was adopted. The two forms were combined to reduce the mutual coupling between antennas and improve the degree of isolation between antennas. In [13], two radiation units were

Received 30 March 2023, Accepted 21 June 2023, Scheduled 11 July 2023
* Corresponding author: Huimei Zhang (1724498568@qq.com).
The authors are with the School of Electronic and Information Engineering, Liaoning Technical University, Huludao 125105, China.

placed orthogonally to use orthogonality decoupling of polarization. Still, the effect could not meet the isolation requirement of the MIMO antenna, so two mutually orthogonal U-shape branches were added on the back of the antenna to improve the isolation between the antennas. In [14], firstly, the mutual coupling between antennas was reduced by increasing the distance between two patch antennas; secondly, T-shape branches were added on the antenna floor to act as reflecting plates to reduce the mutual coupling between antennas further. In [15], two antenna elements were rotated 45 degrees to the left and 45 degrees to the right to make the antenna elements orthogonal to each other, to improve the coupling performance between antennas. In [16], a compact three-band gap complementary split-ring resonator (CTBG-CSRR) unit was proposed, loaded between two microstrip-fed Vivaldi antennas, to reduce the mutual coupling of the three bands in WLAN applications. In [17, 18], neutralization line technology was used to decouple antennas.

In this paper, a four-element UWB MIMO Vivaldi antenna is proposed. T-slots and fence structures are etched into the antenna floor, and I-typed branches are added between radiating ports to increase the isolation degree between antenna units. To ensure the UWB performance of the antenna, resistors and rectangular patch-loading technologies are used. The loaded resistor can absorb the extra electromagnetic wave of the antenna in the low-frequency band so that the antenna bandwidth moves to the low frequency. Loading the rectangular patch as a guide can standardize the main radiation direction of the antenna and improve the antenna impedance matching characteristics; the influence is more evident in the high-frequency band. The working bandwidth of the antenna is $3.0 \sim 12.3$ GHz; the isolation degree in the whole frequency band is greater than 15 dB; and ECC < 0.43, which meets the requirements of the UWB MIMO antenna. The actual test results are in good agreement with the simulation ones.

2. ANTENNA DESIGN AND ANALYSIS

2.1. Antenna Structure

The designed antenna structure is shown in Figure 1. The antenna is printed on an FR4 board with a dielectric constant of 4.4, and the loss tangent value of the dielectric substrate is 0.02. The antenna comprises four Vivaldi antennas arranged in a 2×2 array structure. A 50-ohm microstrip wire feeds each Vivaldi antenna through the design of microstrip wire to slot wire (the feed ports are 1, 2, 3, 4 from top to bottom and from left to right). The front of the antenna comprises four tapered slots, resistors, radiation patches, and decoupling structures, and the back of the antenna consists of four microstrip feeders and I-type branches.

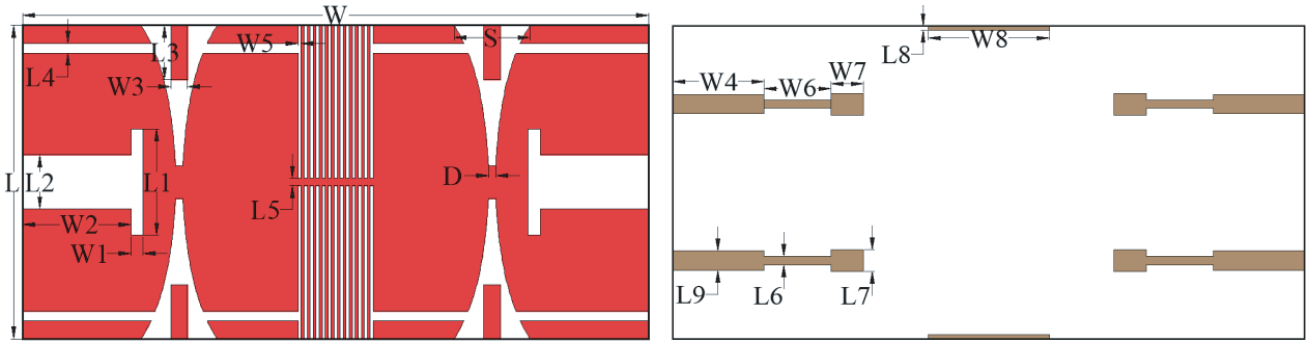

Figure 1. Structure of the antenna. (a) Top view. (b) Bottom view.

The conical curve function of the Vivaldi antenna is as follows [22]:

$$y = \pm \left(C_1 e^{ax} + C_2\right) \tag{1}$$

(x_1, y_1) and (x_2, y_2) are controlled by S and D; $a = 0.2$, a is the curvature of the conical curve, generally

0–1, which determines the bending degree of the conical angle.

$$C_1 = \frac{y_1 - y_2}{e^{ax_2} + e^{ax_1}} \tag{2}$$

$$C_2 = \frac{y_1 e^{ax_2} - y_2 e^{ax_1}}{e^{ax_2} - e^{ax_1}} \tag{3}$$

D determines the antenna's working frequency band's high-frequency point, which should be greater than half of the wavelength corresponding to the high-frequency cutoff frequency. S determines the low frequency of the antenna's operating band, which must be greater than half of the wavelength corresponding to the low-frequency cutoff frequency. Table 1 shows the structural parameters of electromagnetic simulation software HFSS after simulation and optimization.

Table 1. Optimized antenna parameters.

Parameters	W	$W1$	$W2$	$W3$	$W4$	$W5$	$W6$	$W7$	$W8$	S
Value (mm)	52	1	9	1.8	7.5	0.25	5.5	2.7	10	6.3
Parameters	L	$L1$	$L2$	$L3$	$L4$	$L5$	$L6$	$L7$	$L8$	D
Value (mm)	26	8.8	4.5	4.5	0.8	0.6	0.7	1.8	0.35	0.6

2.2. Antenna Design Process

To better understand the antenna structure and facilitate the analysis of antenna parameters, the design process of the four-port MIMO Vivaldi antenna based on resistance and rectangular patch loading is shown in Figure 2. First of all, because the Vivaldi antenna has broadband characteristics, symmetrical

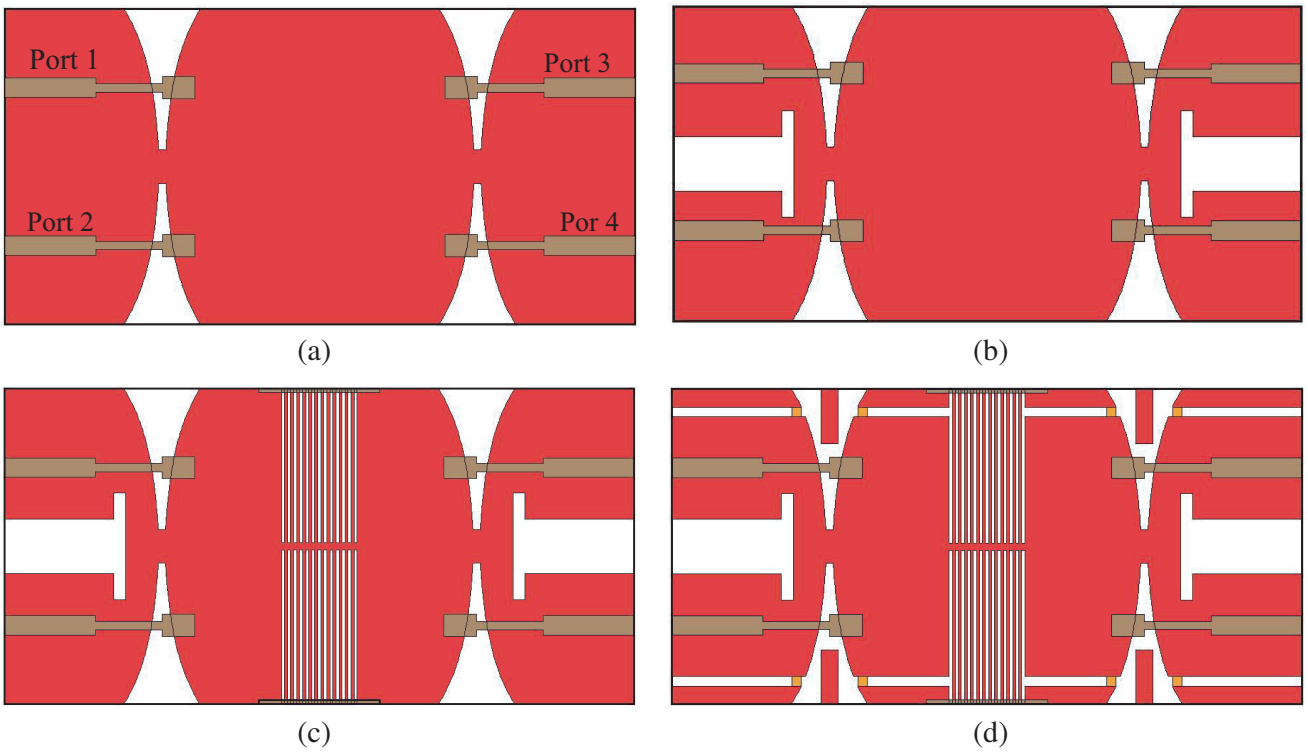

Figure 2. The evolutionary process of designed MIMO antenna. (a) Antenna 1. (b) Antenna 2. (c) Antenna 3. (d) Antenna 4.

radiation pattern, and low cross-polarization, the design chooses to use Vivaldi antenna as the basic unit of the MIMO antenna. It forms a four-port UWB MIMO Vivaldi antenna with 2×2 arrays, as shown in antenna 1. Secondly, to reduce the mutual coupling between antenna elements and improve the isolation performance of the antenna, two T-shape gaps are etched on the antenna floor, as shown in antenna 2. At this time, the isolation between the ports of the antenna is still not ideal, so to further reduce the mutual coupling between the antennas, a fence-type gap is etched on the floor of the antenna, and an I-type branch is loaded on the radiating port, as shown in antenna 3. Finally, to optimize the impedance matching characteristics of the antenna and expand the antenna bandwidth, a resistor is loaded at the opening of the conical gap, and a rectangular radiation patch is loaded in the middle of the conical groove, as shown in antenna 4.

Figure 3 shows the reflection coefficient of each port of antenna 4. The reflection coefficients of each antenna port are lower than -10 dB at 3–12.3 GHz, indicating that the antenna has UWB characteristics and suitable impedance-matching characteristics.

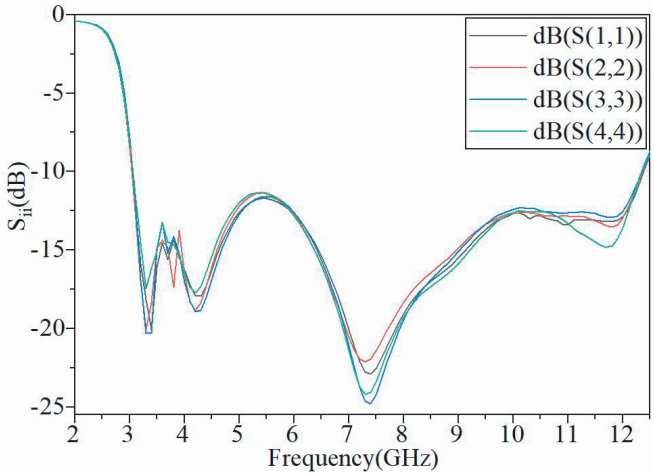

Figure 3. Reflection coefficient of each port. S_{ii} (i is 1, 2, 3, 4).

2.3. Decoupling Design

As shown in Figure 2 for antenna 2 and antenna 3, the decoupled structure of the antenna consists of three parts: T-slot, fence structure, and I-branch. First, a T-slot is etched between the two conical slots in the longitudinal arrangement. The T-slot can increase the current path between the two conical slots, thus reducing the mutual coupling and improving their isolation. At this time, the isolation of each antenna port is improved compared with antenna 1, and especially the isolation between ports 1 and 2 and between ports 3 and 4 is decreased significantly. However, the isolation degree does not meet the isolation requirement of MIMO antenna. Second, a fence structure is etched between two tapered grooves arranged horizontally. From the circuit perspective, these rectangular gaps can be equivalent to a band-stop filter, which shows high impedance characteristics in the UWB MIMO antenna and is crucial in suppressing the mutual coupling of ground surface waves. Therefore, the fence structure can effectively improve antenna isolation. The longitudinal coupling and cross-coupling between the antenna ports have been greatly reduced, but lateral coupling still exists in the low-frequency band. Finally, I-type branches are loaded on the back of the antenna between ports 1 and 3 and between ports 2 and 4. The I-branch creates a current path distributed along this branch, adequately suppressing the current between port 1 and port 3, acting as an isolator.

Figure 4 shows the isolation curves of port 1 and the other three ports. With the addition of the decoupling structure, the mutual coupling between the antennas gradually decreases, and the isolation between the ports gradually increases. It shows that the decoupling structure helps to improve the isolation degree of the designed MIMO antenna. It was eventually concluded that the isolation degree between the MIMO antennas is greater than 15 dB in the whole working frequency band and greater

than 20 dB in the high-frequency band, which meets the isolation requirement of MIMO antennas.

Figure 4 shows the variation curves of port isolation during antenna design. Figure 5 shows the current distribution on the surface of the 4 GHz and 10 GHz MIMO antenna. It can be seen from the figure that when radiation unit 3 is excited, the current is mainly distributed in the radiation

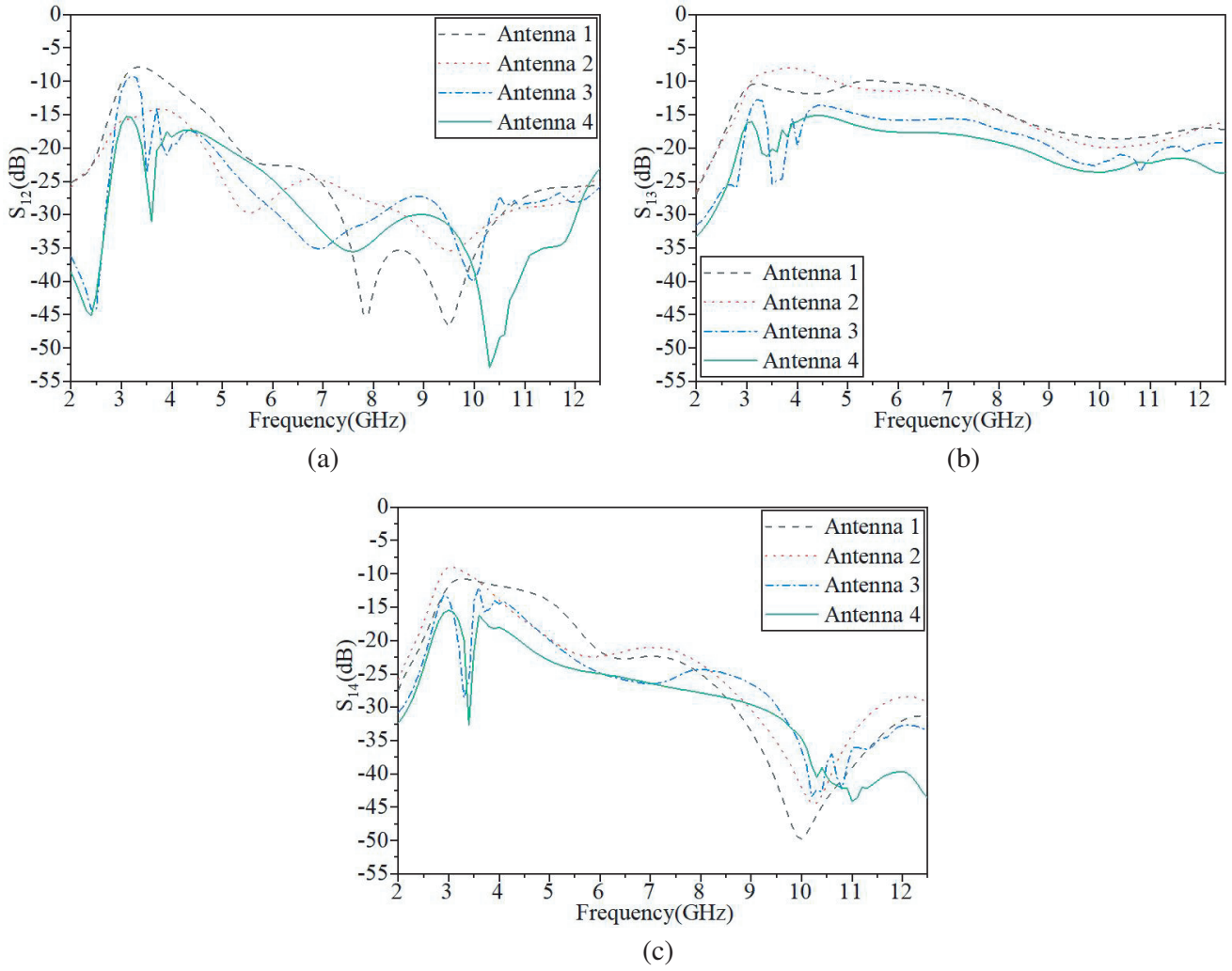

Figure 4. The evolution process of isolation of ports, S_{ij} (i, j is 1, 2, 3, 4). (a) S_{12}. (b) S_{13}. (c) S_{14}.

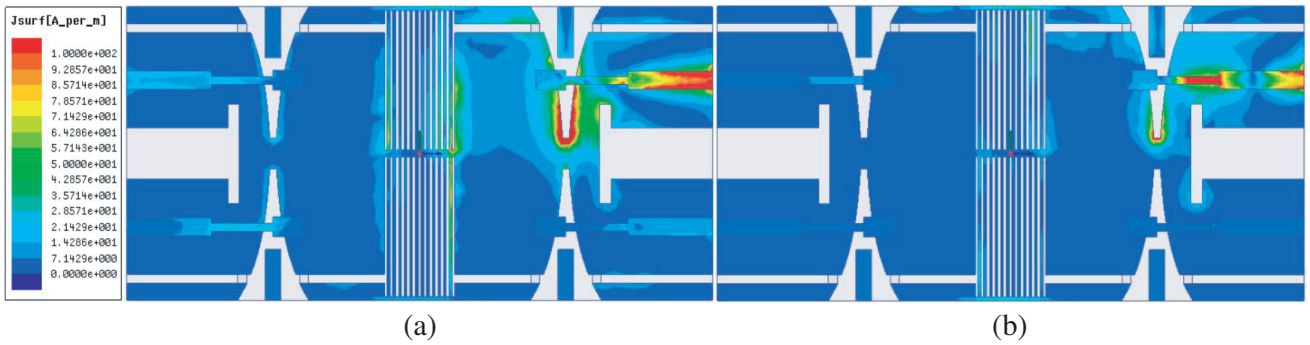

Figure 5. Simulated surface current distribution. (a) 4 GHz. (b) 10 GHz.

unit 3 and its corresponding conical slot, fence structure, edge of the T-slot, and I-type branch. These decoupling structures significantly reduce the coupling between port 3 and other ports so that more energy is coupled to the conical slot corresponding to radiation unit 3, thus improving the transmission performance of the Vivaldi antenna.

2.4. Loading Resistance and Rectangular Radiant Patch

The Vivaldi antenna can expand the antenna bandwidth by changing the structure of the radiation arm [23], resistance loading [24–26], medium loading [27], metal radiation patch loading [28–30], and other methods.

The resistance loading technique is to select the appropriate position in the antenna structure to load the resistance element with a specific resistance value. Generally, the resistance is loaded at the opening of the conical groove or other locations where the current distribution is not concentrated to absorb the excess reflected electromagnetic waves in the low-frequency band, which extends the low-band bandwidth of the antenna. Since the resistance is a lumped element, the radiation efficiency and gain of the antenna will be affected if the resistance value of the loaded resistance is too high or if the resistance is loaded to the place where the current distribution of the antenna is dense. Therefore, the resistance value and loading position should be carefully considered when loading resistance. Figure 6 shows the reflection coefficient of port 2 (the reflection parameters of each port of the MIMO antenna are similar, so one of them is taken to study) graphs under different resistance values loaded based on antenna three. Due to the loading of resistor R, the impedance bandwidth corresponding to port 2 becomes more expansive, and the low-frequency band's impedance characteristics improve progressively. The impedance characteristics of the high-frequency band become worse, and combined with the careful consideration of other antenna performances, it is finally decided that the value of R is 51 ohm.

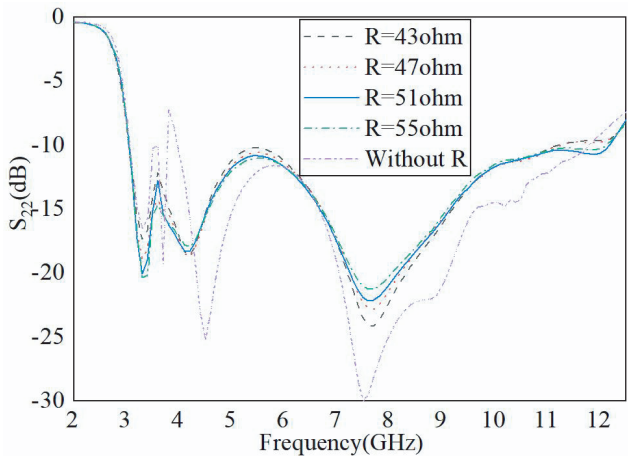

Figure 6. Simulated results of S_{22} with different values of R.

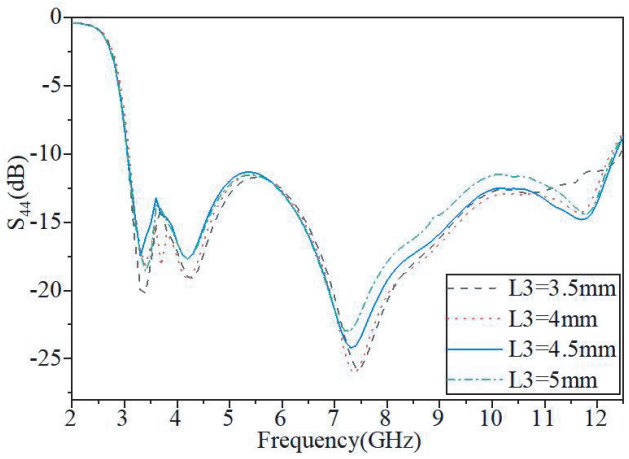

Figure 7. Simulated results of S_{44} with different values of $L3$.

According to the principle of the Yagi antenna metal guide, in the direction of electromagnetic wave propagation, metal objects with specific regular arrangement can play a role in the directional traction of electromagnetic waves. According to this principle, Vivaldi antenna researchers usually load metal patches with particular rules or unique shapes at the opening of the conical slot. Directional traction of electromagnetic waves can regulate the antenna's main radiation direction and improve the antenna's gain and bandwidth in the high-frequency band. As shown in Figure 2 antenna 4, a rectangular metal patch is embedded in the opening of the antenna tapered slot to guide the electromagnetic wave transmission from the aperture of the antenna to the edge of the dielectric plate to avoid unnecessary electromagnetic wave radiation and optimize the transmission characteristics of the antenna. The metal patch's shape, size, and loading position influence the antenna; the common shapes are rectangle,

triangle, oval, composite shape, etc. The antenna uses a rectangular metal patch, and the effect of the length $L3$ of the patch on the antenna impedance bandwidth is studied.

Figure 7 shows the reflection coefficient of port 4 curve of 3–5 mm, and a 0.5 mm step size for $L3$ is taken. With the growth of $L3$, the lowest frequency point hardly moves; the highest frequency point gradually moves to the right; and the reflection coefficient of port 4 curve moves downward.

3. RESULTS AND DISCUSSION

To verify the practicality of the designed UWB MIMO Vivaldi antenna, the actual antenna is fabricated, and its parameters are measured. Figure 8 is a physical antenna picture; the S-parameters of the antenna are measured by connecting the SMA interface with the vector network analyzer. The radiation performance of the antenna was tested in a microwave anechoic chamber. Error in antenna fabrication and measurement is unavoidable, so the simulation and test results cannot match completely. In addition, the antenna needs to weld four SMA connectors and multiple resistors, and the complicated welding process is also a reason for the error.

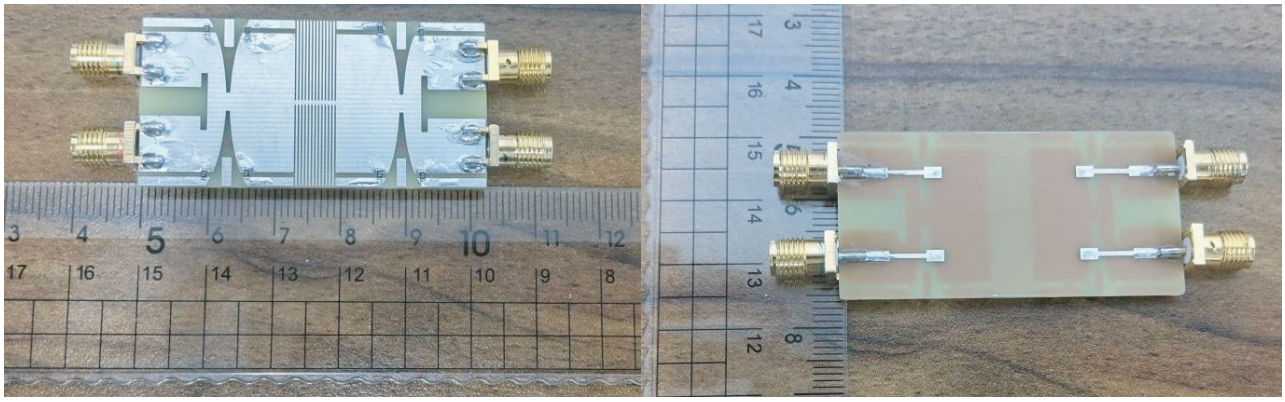

(a) (b)

Figure 8. Fabricated antenna. (a) Top view. (b) Bottom view.

3.1. S-Parameter

Figure 9 is the antenna S parameter diagram, from which it can be seen that the simulation curve is consistent with the measurement curve. The measured antenna impedance bandwidth is $3.0 \sim 12.3$ GHz; $S_{11} < -10$ dB; antenna isolation is > 15 dB in the whole working bandwidth; and high-frequency band isolation is > 20 dB. The antenna has good impedance characteristics and port isolation.

3.2. Radiation Pattern

Figure 10 shows the radiation patterns simulated and tested at 4, 6.8, and 10 GHz when the designed MIMO antenna port 1 is excited. The consistency between the simulated and measured radiation patterns verifies the correctness of the design. The experimental results show that the antenna has good radiation performance.

3.3. Diversity Analysis

Diversity characteristics are essential for MIMO antennas and can be evaluated by the envelope correlation coefficient (ECC) and diversity gain (DG). In general, ECC must be very small to obtain better antenna diversity characteristics and increase the degree of independence of received information between antenna units. The ideal ECC value is 0, and the ECC is generally less than 0.5 for MIMO antennas. DG is also an important parameter that shows the effect of the diversity scheme of the

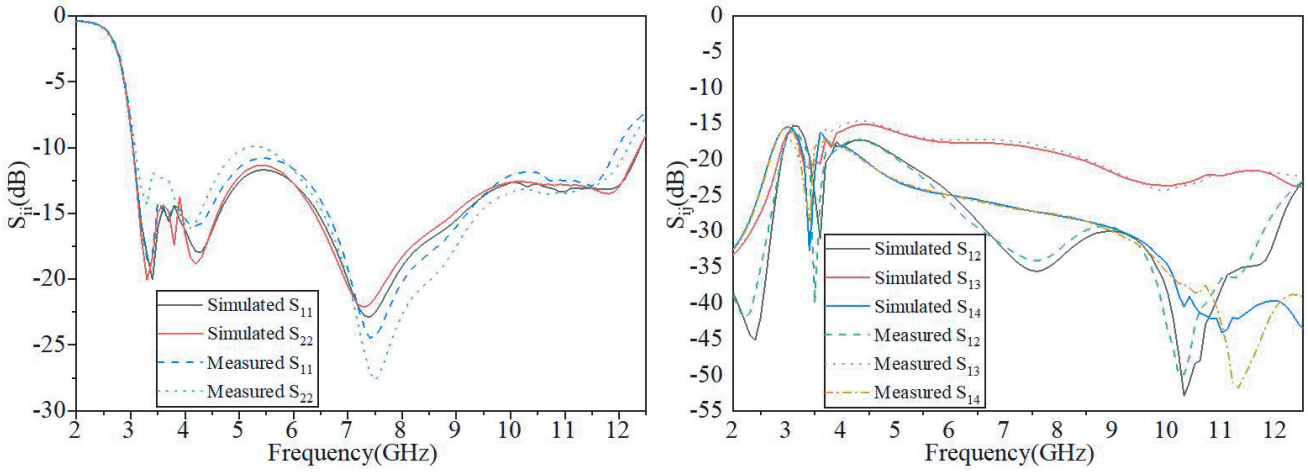

Figure 9. Simulated and measured S-parameter of designed antenna. (a) S_{ii}. (b) S_{ij}.

MIMO antenna on the radiated power. The equations for calculating ECC (ρ_{eij}) and DG using far-field radiation and S parameters are as follows [31–33]:

$$\rho_{eij} = \frac{\left| \int \int_0^{4\pi} \left[\vec{R}_i(\theta,\phi) \times \vec{R}_j(\theta,\phi) \right] d\Omega \right|^2}{\int \int_0^{4\pi} \left| \vec{R}_i(\theta,\phi) \right|^2 d\Omega \int \int_0^{4\pi} \left| \vec{R}_j(\theta,\phi) \right|^2 d\Omega} \tag{4}$$

$$\rho e(i,j,N) = \frac{\left| \sum_{n=1}^{N} S_{i,n}^* S_{n,j} \right|^2}{\prod_{k=(i,j)} \left[1 - S_{i,n}^* S_{n,k} \right]} \tag{5}$$

$$DG = 10 \times \sqrt{1 - |\rho_{eij}|^2} \tag{6}$$

The ECC and DG based on far-field radiation calculations are shown in Figure 11 (According to the specificity of the arrangement structure of the designed antenna, only the relationship between port 1 and the other three ports needs to be studied here.). In the entire impedance bandwidth, ECC < 0.43, DG > 9.65 dBi, indicating that the MIMO antenna has outstanding characteristics with low correlation and high diversity gain.

3.4. Total Active Reflection Coefficient

For MIMO systems, adjacent antenna units affect each other and may affect the overall working bandwidth and efficiency. To account for this effect, a new index is introduced as the total active reflection coefficient (TARC). Standard four-port MIMO systems can be described by Formulas (7) and (8) [34, 35].

$$TRAC = \frac{\sqrt{\sum_{i=1}^{N} \left| S_{i1} + \sum_{m=2}^{N} S_{im} e^{j\theta_{m-1}} \right|^2}}{\sqrt{N}} \tag{7}$$

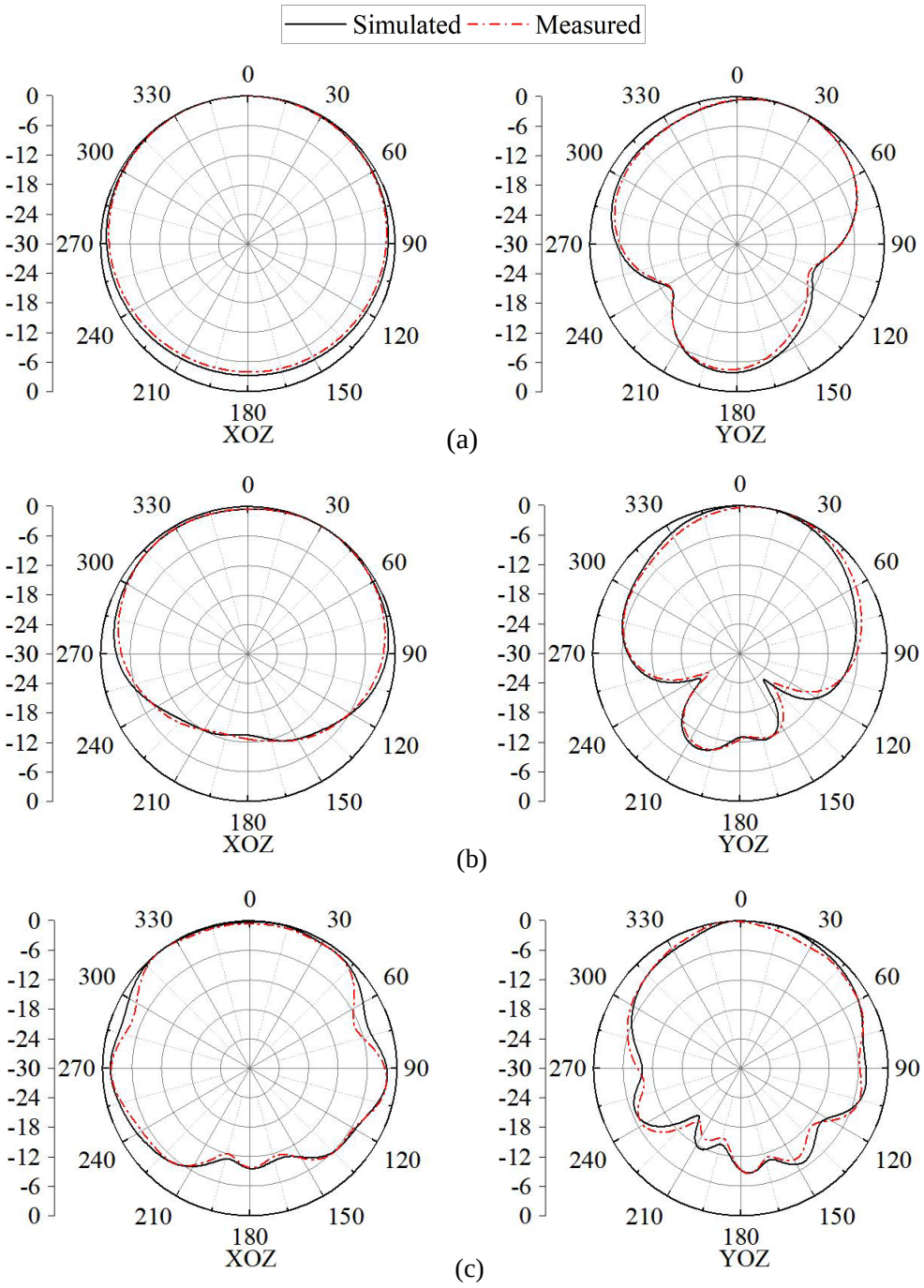

Figure 10. Simulated and measured results of radiation patterns. (a) 4 GHz. (b) 6.8 GHz. (c) 10 GHz.

$$TARC = \frac{\sqrt{\begin{array}{l}\left|S_{11}+S_{12}e^{j\theta_1}+S_{13}e^{j\theta_2}+S_{14}e^{j\theta_3}\right|^2+\left|S_{21}+S_{22}e^{j\theta_1}+S_{23}e^{j\theta_2}+S_{24}e^{j\theta_3}\right|^2\\ +\left|S_{31}+S_{32}e^{j\theta_1}+S_{33}e^{j\theta_2}+S_{34}e^{j\theta_3}\right|^2+\left|S_{41}+S_{42}e^{j\theta_1}+S_{43}e^{j\theta_2}+S_{44}e^{j\theta_3}\right|^2\end{array}}}{\sqrt{4}} \quad (8)$$

The TRAC results calculated with signals of different phases in the input are shown in Figure 12. There is a slight variation in bandwidth and resonant frequency, but the obtained results are still considered suitable for the intended application of optimal MIMO performance.

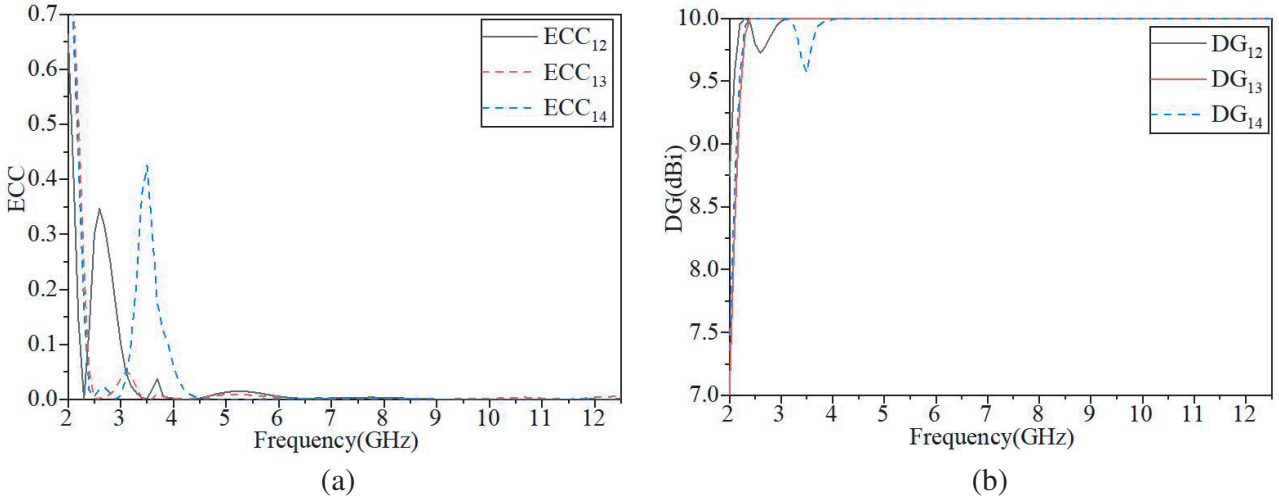

Figure 11. Simulated and measured results of ECC and DG. (a) ECC. (b) DG.

3.5. Antenna Radiation Efficiency

The radiation efficiency of the antenna is shown in Figure 13. It can be observed that the radiation efficiency over the whole working bandwidth is about 75% and up to 91%. But the radiation efficiency of the low-frequency band is not ideal, possibly because of the effect of electrical resistance.

3.6. Comparison with Related Works

Table 2 compares the antenna designed in this paper with related works in the references. The antenna as a four-port antenna is very advantageous in size, and the bandwidth and isolation of this antenna in a relatively compact structure can also meet the requirements of the MIMO antenna system well. It shows the practicality of the designed antenna.

Table 2. Comparison of the designed antenna with previous work.

Ref.	Number of ports	Isolation Improvement Techniques	Overall Siza (mm^3)	Operating bands (GHz)	Min. Isolation (dB)	ECC	Diversity Gain (dBi)
[4]	2	Slotted ground plane	$48 \times 31 \times 1.6$	2.28–2.47 3.34–3.73 4.57–6.75	20	0.002	9.998
[8]	4	Parasitic decoupler	$60 \times 60 \times 1.52$	3–12.8	21	0.001	10
[9]	2	T-shaped stub	$42 \times 30 \times 0.79$	2.8–4.9 5.4–11	20	0.03	10
[10]	2	Fence-typed structure	$50 \times 35 \times 1$	3–11	25	0.004	–
[12]	2	ITI-shaped structure	$72 \times 56 \times 0.8$	2.24–2.90 3.9–7.55	24	0.04	9.95
This work	4	Hybrid decoupling structure	$26 \times 52 \times 0.8$	$3.0 \sim 12.3$	15	0.43	10

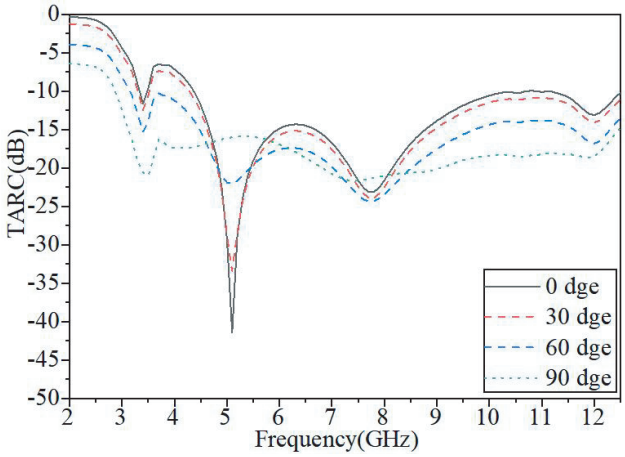

Figure 12. Simulated and measured results of TARC.

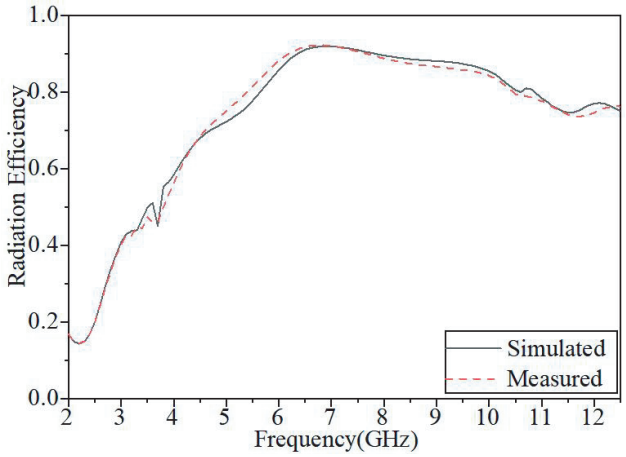

Figure 13. Simulated and measured results of radiation efficiency.

4. CONCLUSION

In this paper, a four-port MIMO Vivaldi antenna is proposed. The antenna takes the Vivaldi antenna as the basic unit and is arranged in a 2×2 array. The antenna size of the compact structure is only 26 mm $\times$ 52 mm $\times$ 0.8 mm. Load resistance to extend the antenna's low-frequency bandwidth at the antenna taper slot opening. The antenna's main radiation direction and high frequency are optimized by loading a rectangular radiation patch in the middle of the cone groove. The hybrid method is used to decouple the antenna and make it have a good isolation degree. The experimental structure shows that the working bandwidth of the antenna is $3.0 \sim 12.3$ GHz. The isolation between the antenna ports is higher than 15 dB in the whole frequency band, but the isolation between port 1 and port 2 and between port 1 and port 4 is higher than 20 dB in the high-frequency band. The envelope correlation coefficient ECC < 0.43, and the antenna has good diversity gain. In conclusion, the antenna has good radiation performance and stable gain, which is suitable for the application to UWB MIMO systems.

ACKNOWLEDGMENT

This work was supported by the National Natural Science Foundation of China under Grant No. 61971210.

REFERENCES

1. Srivastava, G. and M. Khari, "An elliptical CPW fed UWB slot antenna," *Wireless Personal Communications*, Vol. 119, No. 10, 2253–2263, 2021.
2. Kundu, S., "Experimental study of a printed ultra-wideband modified circular monopole antenna," *Microwave and Optical Technology Letters*, Vol. 61, No. 10, 1388–1393, 2019.
3. Marchais, C., G. le Ray, and A. Sharaiha, "Stripline slot antenna for UWB communications," *IEEE Antennas and Wireless Propagation Letters*, Vol. 5, No. 1, 319–322, 2006.
4. Bayarzaya, B., N. Hussain, W. A. Awan, M. A. Sufian, A. Abbas, D. Choi, J. Lee, and N. Kim, "A compact MIMO antenna with improved isolation for ISM, sub-6 GHz, and WLAN application," *Micromachines*, Vol. 13, No. 8, 1355, 2022.
5. Najam, A., Y. Duroc, and S. Tedjni, "UWB-MIMO antenna with novel stub structure," *Progress In Electromagnetics Research C*, Vol. 19, 245–257, 2011.

6. Wani, Z. and D. Kumar, "Dual-band-notched antenna for UWB MIMO applications," *International Journal of Microwave and Wireless Technologies*, Vol. 9, No. 2, 381–386, 2017.
7. Najafy, V. and M. Bemani, "Mutual-coupling reduction in triple-band MIMO antennas for WLAN using CSRRs," *International Journal of Microwave and Wireless Technologies*, Vol. 12, No. 8, 762–768,2020.
8. Abbas, A., N. Hussain, M. A. Sufian, J. Jung, S. M. Park, and N. Kim, "Isolation and gain improvement of a rectangular notch UWB-MIMO antenna," *Sensors*, Vol. 22, No. 4, 1460, 2022.
9. Yadav, D., M. P. Abegaonkar, S. K. Koul, V. Tiwari, and D. Bhatnagar, " Two element band-notched UWB MIMO antenna with high and uniform isolation," *Progress In Electromagnetics Research M*, Vol. 63, 119–129, 2018.
10. Wang, L., Z. Du, H. Yang, R. Ma, Y. Zhao, X.Cui, and X. Xi, "Compact UWB MIMO antenna with high isolation using fence-type decoupling structure," *IEEE Antennas and Wireless Propagation Letters*, Vol. 18, No. 8, 1641–1645, 2019.
11. Li, Z., C. Yin, and X. Zhu, "Compact UWB MIMO Vivaldi antenna with dual band-notched characteristics," *IEEE Access*, Vol. 7, 38696–38701, 2019.
12. Kumar, A., A. Q. Ansari, B. K. Kanaujia, and J. Kishor, "A novel ITI-shaped isolation structure placed between two-port CPW-fed dual-band MIMO antenna for high isolation," *AEU — International Journal of Electronics and Communications*, Vol. 104, 35–43, 2019.
13. Tang, Z., J. Zhan, X. Wu, Z. Xi, L. Chen, and S. Hu, "Design of a compact UWB-MIMO antenna with high isolation and dual band-notched characteristics," *Journal of Electromagnetic Waves and Applications*, Vol. 34, No. 4, 500–513, 2020.
14. Arma, M., "Design and analysis of MIMO antenna with high isolation and dual notched band characteristics for wireless applications," *Wireless Personal Communications*, Vol. 112, No. 3, 1587–1599, 2020.
15. Elabd, R. H., H. H. Abdullah, and M. Abdelazim, "Compact highly directive MIMO Vivaldi antenna for 5G millimeter-wave base station," *Journal of Infrared, Millimeter, and Terahertz Waves*, Vol. 42, No. 2, 173–194, 2021.
16. Najafy, V. and M. Bemani, "Mutual-coupling reduction in triple-band MIMO antennas for WLAN using CSRRs," *International Journal of Microwave and Wireless Technologies*, Vol. 12, No. 8, 762–768, 2020.
17. Tiwari, R. N., P. Singh, and B. K. Kanaujia, "A compact UWB MIMO antenna with neutralization line for WLAN/ISM/mobile applications," *International Journal of RF and Microwave Computer-Aided Engineering*, Vol. 29, No. 11, e21907, 2019.
18. Zhang, S. and G. F. Pedersen, "Mutual coupling reduction for UWB MIMO antennas with a wideband neutralization line," *IEEE Antennas and Wireless Propagation Letters*, Vol. 15, 166–169, 2016.
19. Kumar, A., A. Q. Ansari, B. K. Kanaujia, J. Kishor, and L. Matekovits, "A review on different techniques of mutual coupling reduction between elements of any MIMO antenna. Part 1: DGSs and parasitic structures," *Radio Science*, Vol. 56, No. 3, 1–25, 2021.
20. Kumar, A., A. Q. Ansari, B. K. Kanaujia, J. Kishor, and L. Matekovits, "A review on different techniques of mutual coupling reduction between elements of any MIMO antenna. Part 2: Metamaterials and many more," *Radio Science*, Vol. 56, No. 3, 2021.
21. Bhattacharjee, A., A. Karmakar, and A. Saha, "A compact UWB DRA MIMO antenna realizing band notch characteristics and fractal inspired isolation mechanism," *Progress In Electromagnetics Research C*, Vol. 123, 213–226, 2022.
22. Gibson, P. J., "The vivaldi aerial," *IEEE 9th European Microwave Conference*, 101–105, Brighton, UK, September 1979.
23. De Oliveira, A. M., M. B. Perotoni, S. T. Kofuji, and J. F. Justo, "A palm tree Antipodal Vivaldi Antenna with exponential slot edge for improved radiation pattern," *IEEE Antennas and Wireless Propagation Letters*, Vol. 14, 1334–1337, 2015.

24. Deng, C. and Y. J. Xie, "Design of resistive loading Vivaldi antenna," *IEEE Antennas and Wireless Propagation Letters*, Vol. 8, 240–243, 2009.
25. Chen, M. Z., H. B. Wang, and Y. J. Cheng, "2–18 GHz balanced antipodal Vivaldi conformal phased array antenna with resistive load and shorting posts," *International Journal of RF and Microwave Computer-Aided Engineering*, Vol. 32, No. 11, 2022.
26. Zhao, C., X. Li, M. Yang, and C. Sun, "Resistance-loaded miniaturized dual-layer Vivaldi antenna for plasma reflection diagnosis," *Microwave and Optical Technology Letters*, Vol. 63, No. 1, 205–210, 2012.
27. Huang, M., L. Wang, and W. Qiao, "Design of 2 to 18 GHz balanced antipodal Vivaldi antennas using substrate-integrated lenses," *Electromagnetics*, Vol. 38, No. 7, 478–487, 2018.
28. Nassar, I. T. and T. M. Weller, "A novel method for improving antipodal Vivaldi antenna performance," *IEEE Transactions on Antennas and Propagation*, Vol. 63, No. 7, 3321–3324, 2015.
29. Wang, W. and Y. Zheng, "Improved design of the vivaldi dielectric notch radiator with etched slots and a parasitic patch," *IEEE Antennas and Wireless Propagation Letters*, Vol. 17, No. 6, 1064–1068, 2018.
30. Kumar Jaiswal, P., R. Bhattacharya, and A. Kumar, "A UWB Antipodal Vivaldi antenna with high gain using metasurface and notches," *AEU — International Journal of Electronics and Communications*, Vol. 159, 154473, 2023.
31. Aghoutane, B., S. Das, M. el Ghzaoui, B. T. P. Madhav, and H. el Faylali, "A novel dual band high gain 4-port millimeter wave MIMO antenna array for 28/37 GHz 5G applications," *AEU — International Journal of Electronics and Communications*, Vol. 145, 154071, 2022.
32. Kumar, A., A. Q. Ansari, B. K. Kanaujia, J. Kishor, and S. Kumar, " An ultra-compact two-port UWB-MIMO antenna with dual band-notched characteristics," *AEU — International Journal of Electronics and Communications*, Vol. 114, 154071, 2020.
33. Kumar, A., G. Saxena, P. Kumar, Y. K. Awasthi, P. Jain, S. S. Singhwal, and P. Ranjan, "Quad-band circularly polarized super-wideband MIMO antenna for wireless applications," *International Journal of RF and Microwave Computer-Aided Engineering*, Vol. 32, No. 6, e23129, 2022.
34. Kumar, A., A. Q. Ansari, B. K. Kanaujia, and J. Kishor, "High isolation compact four-port MIMO antenna loaded with CSRR for multiband applications," *Frequenz*, Vol. 72, No. 9–10, 415–427, 2018.
35. Sufian, M. A., N. Hussain, A. Abbas, J. Lee, S. G. Park, and N. Kim, "Mutual coupling reduction of a circularly polarized MIMO antenna using parasitic elements and DGS for V2X communications," *IEEE Access*, Vol. 10, 56388–56400, 2022.